The Temperature and Pressure Dependence of the Reactions H + O_2 (+M) → HO_2 (+M) and H + OH (+M) → H_2O (+M)

Stig R. Sellevåg,*,† Yuri Georgievskii,‡ and James A. Miller*,‡

SINTEF Energy Research, NO-7465 Trondheim, Norway and Combustion Research Facility, Sandia National Laboratories, Livermore, California 94551-0969, USA

Received: December 16, 2007; Revised Manuscript Received: February 21, 2008

The reactions H + O_2 (+M) → HO_2 (+M) and H + OH (+M) → H_2O (+M) have been studied using high-level quantum chemistry methods. On the basis of potential energy hypersurfaces obtained at the CASPT2/aug-cc-pVTZ level of theory, high-pressure limiting rate coefficients have been calculated using variable reaction coordinate transition state theory. Over the temperature range 300−3000 K, the following expressions were obtained in units of cm^3 $molecule^{-1}$ s^{-1}: $k_\infty(H + O_2) = (25T^{-0.367} + (7.5 \times 10^{-2})T^{0.702}) \times 10^{-11}$ and $k_\infty(H + OH) = (4.17 \times 10^{-11})T^{0.234}\exp(57.5/T)$. Available experimental data on the pressure dependence of the reactions were analyzed using a two-dimensional master equation. The following low-pressure limiting rate coefficients were obtained over the temperature range 300−3000 K in units of cm^6 $molecule^{-2}$ s^{-1}: $k_0(H + O_2 + Ar) = (9.1\times10^{-29})T^{-1.404}\exp(-134/T)$, $k_0(H + O_2 + N_2) = (2.0\times10^{-27})T^{-1.73}\exp(-270/T)$, $k_0(H + OH + Ar) = (8.6\times10^{-28})T^{-1.527}\exp(-185/T)$, and $k_0(H + OH + N_2) = (1.25\times10^{-26})T^{-1.81}\exp(-251/T)$. For the H + O_2 reaction system, $F_{cent}(Ar) = 0.67$ and $F_{cent}(N_2) = 0.72$ were obtained as center broadening factors, whereas $F_{cent}(Ar) = 0.72$ and $F_{cent}(N_2) = 0.73$ were obtained for the H + OH reaction system. The calculations provide a good description of most of the experimental data, except the room temperature measurements on the H + OH (+M) → H_2O (+M) reaction.

1. Introduction

Today it is evident that use of fossil fuels has contributed to an unequivocal warming of the climate system.[1] Use of hydrogen (H_2) manufactured from natural gas or coal to create "decarbonized fuels" has the potential to significantly reduce CO_2 emissions from the power production industry. To use H_2 as gas turbine fuel, an accurate description of the combustion process at elevated pressures is needed. However, even apparently small differences between the available chemical mechanisms for H_2 combustion can have a significant effect on predicted flame properties.[2–4] Thus, although significant progress has been made to provide a detailed description of the chemical kinetics involved at these conditions,[5] some uncertainties still remain. To help improve the chemical insight into the combustion of H_2, we have initiated a quantum chemistry study of some pressure-dependent elementary chemical reactions involved at conditions relevant for gas turbines.

The reaction

$$H(^2S) + O_2(X^3\Sigma_g^-)(+M) \rightarrow HO_2(X^2A'')(+M) \qquad (1)$$

is an important chain-terminating reaction in combustion. Few experimental studies of the high-pressure limiting rate coefficient, $k_\infty(T)$, for reaction 1 have been reported. On the basis of extrapolation of falloff curves, Cobos et al.[6] reported $k_{1,\infty} \simeq 7.5\times10^{-11}(T/300\ K)^{0.6}$ cm^3 $molecule^{-1}$ s^{-1}. Bates et al.[7] reported $k_{1,\infty} = 4.7\times10^{-11}(T/300\ K)^{0.2}$ cm^3 $molecule^{-1}$ s^{-1} based on Rice−Ramsperger−Kassel−Marcus (RRKM) analysis of data obtained at elevated pressures; however, as stated by Bates and colleagues, the RRKM model prediced a somewhat larger rate compared to the experiments at the highest pressures when argon was used as bath gas. The fit of the experimental data of Hahn et al.[8] obtained over the ranges 1−900 bar and 300−700 K, was consistent with the high-pressure limiting rate coefficient preferred by the IUPAC panel,[9] $9.5\times10^{-11}(T/300\ K)^{0.44}$ cm^3 $molecule^{-1}$ s^{-1}.

There have been numerous experimental studies of the low-pressure limiting rate coefficient, k_0, and the falloff behavior of reaction 1. For brevity we refer to Baulch et al.[9] for a review. The IUPAC preferred values[9] for $k_{1,0}/cm^6$ $molecule^{-2}$ s^{-1} are $1.9\times10^{-29}T^{-1.2}$ for M = Ar and $7.3\times10^{-29}T^{-1.3}$ for M = N_2 over the temperature range 298−2000 K. The IUPAC preferred values for the center broadening factor, F_{cent}, are 0.51 for M = Ar and 0.57 for M = N_2 over the temperature range 298−1500 K.

Several theoretical studies of $k_{1,\infty}$ have been reported.[10–14] On the basis of classical trajectory calculations carried out on a two-dimensional potential energy hypersurface (PES) obtained at the CAS+1+2+QC/aug-cc-pVTZ level of theory, Harding et al.[10,11] obtained $k_{1,\infty} = 9.5\times10^{-11}(T/300\ K)^{0.44}$ cm^3 $molecule^{-1}s^{-1}$ over the temperature range 300−2000 K. As mentioned above, this value forms the basis for the preferred value of the IUPAC panel.[9] Harding and co-workers also obtained energy (E) and total angular momentum (J) specific rate coefficients, $k(E, J)$, for reaction 1. Lin et al.[14] have calculated $k_{1,\infty}$ using a time-independent quantum capture method. These calculations were performed on the DMBE IV[15] potential energy surface, which has received some criticism for not providing an accurate description of the parts of the potential that are important for the kinetics.[10,16]

Several groups[11,17–21] have theoretically investigated the falloff behavior of reaction 1. Teitelbaum et al.[17] obtained lifetime distributions of the HO_2 complex as a function of vibrational quantum number and temperature based on classical trajectory

* Authors to whom correspondence should be addressed. E-mail: s.r.sellevag@kjemi.uio.no (S.R.S); jamille@sandia.gov (J.A.M.).
† SINTEF Energy Research.
‡ Sandia National Laboratories.

10.1021/jp711800z CCC: $40.75
Published on Web 05/21/2008

TABLE 1: Electronic (D_e) and Bond (D_0) Dissociation Energies (at 0 K) of the H−O_2 Bond of the HO_2 (X^2A'') Radical

method[a]	D_e/kcal mol^{-1}	D_0/kcal mol^{-1} harmonic	D_0/kcal mol^{-1} anharmonic
B3LYP/aTZ	54.3	47.8	
MP2/aTZ	45.1	38.1	38.5
CCSD(T)/aTZ//MP2/aTZ	53.7	46.7	47.1
CCSD(T)/aQZ//MP2/aTZ	54.5	47.6	47.9
CCSD(T)/a5Z//MP2/aTZ	54.7	47.8	48.2
CCSD(T)/EBQT//MP2/aTZ	55.2	48.2	48.6
CCSD(T)/EB5Q//MP2/aTZ	55.0	48.0	48.4
CASPT2/aTZ	44.1	37.6	
CASPT3/aTZ//CASPT2/aTZ	62.5	55.9	
CAS+1+2+QC/aTZ[b]	51.2	44.4	
experiment[c]			47.99 ± 0.06

[a] Abbreviations: aXZ = aug-cc-pVXZ; EB XY = basis set extrapolation of aug-cc-pVXZ and aug-cc-pV YZ where $Y = X-1$, see eq 3. [b] See Harding et al.[10] [c] See Ruscic et al.[63]

calculations performed on the DMBE IV PES.[15]Teitelbaum and co-workers also calculated falloff curves for reaction 1 with Ar as a third body using the factorization scheme of Troe.[22] Troe's factorization scheme was also used by Michael et al.[18] to analyze their experimental low-pressure data. On the basis of data obtained by Harding et al.,[10] Troe[11] has constructed complete falloff curves for reaction 1 over the temperature range 300−2000 K. Troe[11] concluded that, because the dynamics of the reaction were neither adiabatic nor sudden, approaches based on RRKM theory or the simplified statistical adiabatic channel model (SACM) do not provide a proper description of the reaction system. Using the DMBE IV PES,[15] Himmer and Roduner[19] investigated the pressure dependence of reaction 1 within RRKM theory. RRKM calculations have also been carried out by Duchovic et al.[20] using ab initio data obtained by Walch and co-workers.[23–25] Mandelshtam et al.[21] have calculated $k_{1,0}$ using quantum dynamics with filter diagonalization on the DMBE IV potential energy surface. However, the calculations were done within the strong collision approximation. For brevity we refer to Duchovic et al.[20] for a summary of earlier studies.

The recombination of hydrogen atoms and hydroxyl radicals to form water (eq 2) is of importance for describing laminar flame speeds, especially at elevated pressures.[2,3,26]

$$H(^2S) + OH(X^2\Pi)(+M) \rightarrow H_2O(X^1A_1)(+M) \qquad (2)$$

Several experimental studies of $k_{2,0}$ have been reported in the literature; see Baulch et al.[9] for a review. The current IUPAC preferred values of the low-pressure limiting rate coefficient are $k_{2,0} = 2.3\times10^{-26}T^{-2.0}$ cm^6 molecule^{-2} s^{-1} for M = Ar and $k_{2,0} = 6.1\times10^{-26}T^{-2.0}$ cm^6 molecule^{-2} s^{-1} for M = N_2 over the temperature range 300−3000 K;[9] however, the data are badly scattered. Recently, Srinivasan and Michael[27] have experimentally investigated the thermal decomposition of water. They reported $k_{-2,0} = (2.43 \pm 0.57)\times10^{-10}\exp[-(47117 \pm 633)/T]$ cm^3 molecule^{-1} s^{-1} for Kr or Ar as bath gas. To our knowledge, no experimental data on $k_{2,\infty}$ or the falloff behavior of reaction 2 have been reported in the literature.

Several studies have theoretically investigated long-range interactions within the water molecule.[28–31] The focus has, however, been on the competing $O(^1D) + H_2(X^1\Sigma_g^+) \rightarrow OH(X^2\Pi) + H(^2S)$ reaction. As far as we know, only two theoretical studies of reaction 2 have been reported: the high-pressure limiting rate coefficient has been calculated by Cobos and Troe[32] using the simplified statistical adiabatic channel model, and Troe[33] investigated the low-pressure limit by assuming strong collisions. The understanding of this reaction is, thus, unsatisfactory.

In this work we have employed large basis set, ab initio calculations together with variable reaction coordinate transition state theory incorporating multifaceted dividing surface (VRC-TST)[34,35] to calculate high-pressure limiting rate coefficients for the reactions under study. The low-pressure limiting rate coefficients and the falloff behavior of the reactions were investigated using a two-dimensional master equation.

2. Computational Methods

2.1. Electronic Structure Calculations. Ground-state potential energy hypersurfaces (PES) of reactions 1 and 2 were investigated using the complete active space self-consistent field (CASSCF) method of Knowles and Werner.[36,37] Dynamical electron correlation was included using the complete active space second-order (CASPT2) and third-order (CASPT3) perturbation theory methods of Werner[38] and using the internally contracted multireference configuration-interaction (MRCI) method of Werner and Knowles[39,40] with single and double excitations and CASSCF reference space (CAS+1+2). The CASPT2, CASPT3, and CAS+1+2 calculations used identical CASSCF reference spaces. The CAS+1+2 calculations also included a multireference Davidson correction to correct for the neglect of higher-order excitations, hereafter abbreviated as CAS+1+2+QC. The active space used to describe the H + O_2 reaction system consisted of seven electrons in five orbitals; the selected orbitals were the hydrogen 1s orbital and the O_2 π and π^* orbitals. This active space is identical to that used by Harding et al.[10] For the H + OH reaction system, the active space consisted of four electrons in three orbitals; the selected orbitals were the σ and σ^* orbitals of the O−H bond being formed and one p orbital on oxygen. Reference energies of reactants were obtained using a supermolecule approach. Spin−orbit (SO) matrix elements were computed for the H + OH reaction system using the Breit−Pauli Hamiltonian. Wavefunctions for the spin−orbit states were generated using MRCI with reference CASSCF configurations only. The CASSCF, CAS+1+2, CASPT2, and CASPT3 calculations were carried out using the MOLPRO package.[41]

Additional calculations were carried out with the Becke 3 parameter[42] Lee−Yang−Parr[43] (B3LYP) hybrid functional, Møller−Plesset second-order perturbation theory (MP2),[44] and coupled-cluster singles and doubles theory with perturbational triples corrections [CCSD(T)].[45] Unrestricted wavefunctions for singlet states were generated by mixing the HOMO and LUMO orbitals in the initial guess. The B3LYP and CCSD(T) calculations were carried out using the Gaussian 98 suite of programs.[46] Anharmonic zero-point vibrational energies (ZPE) of stationary points were calculated using the MP2 model implemented in GAMESS.[47,48]

Dunning's correlation-consistent aug-cc-pVXZ (X = D, T, Q, 5)[49–51] basis sets were employed in all calculations except in the calculation of the SO matrix elements where the Pople-style 6-311++G(3df,p) basis set was used. Single-point correlation energies were extrapolated toward the basis-set limit using the extrapolation scheme of Halkier et al. (eq 3);[52]

$$E_{XY}^{\infty} = \frac{X^3E_X - Y^3E_Y}{X^3 - Y^3} \qquad (3)$$

where E_X is the correlation energy obtained with the highest cardinal number X, and $E_Y$is the correlation energy obtained with cardinal number $Y = X-1$. In the following, such

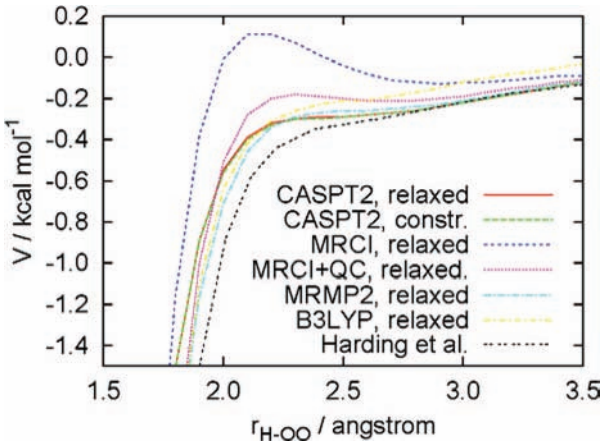

Figure 1. Minimum energy path for the reaction H + O_2 → HO_2 (X^2A'') as a function of the H−O_2 bond length, r_{H-OO}, as calculated using several levels of theory employing the aug-cc-pVTZ basis set with relaxed and constrained HO−O bond length, r_{HO-O}. Here, MRCI denotes the CAS+1+2 method; see text for details. The result of Harding et al.[10] was computed using the CAS+1+2+QC/aug-cc-pVTZ model with relaxed r_{HO-O}. The energies are relative to the energy of the reactants and include electronic energy only.

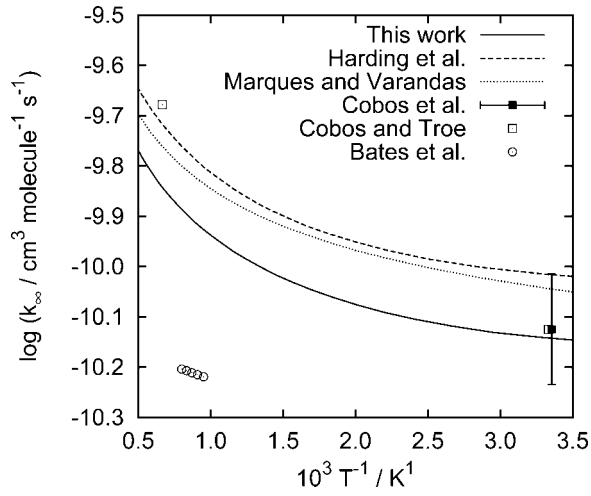

Figure 2. High-pressure limiting rate coefficient (k_∞) as a function of temperature (T) for the reaction H + O_2 → HO_2 (X^2A''). References: Marques and Varandas,[12,71] Harding et al.,[10] Cobos et al.,[6] Cobos and Troe,[32] and Bates et al.[7]

calculations will be referred to, for example, as CCSD(T)/EB *XY* with "EB" being short for extrapolated basis.

2.2. Calculation of High-Pressure Limiting Rate Coefficients. The rate coefficient for the recombination reaction in the high-pressure limit at a given temperature T was calculated from the equation 4,[53]

$$k_\infty(T) = \frac{1}{2\pi} f_{el}\left(\frac{\sigma_A\sigma_B}{\sigma^\dagger}\right)\left(\frac{2\pi}{\mu k_B T}\right)^{3/2} \times \frac{\int N^\dagger(E,\ J)\exp(-E/k_BT)\,\mathrm{d}E\,\mathrm{d}J}{Q_A(T)Q_B(T)} \quad (4)$$

where the labels "A", "B", and "†" denote that the quantities are for reactant A, reactant B, and the transition state (TS), respectively. Here, k_B is the Boltzmann constant, f_{el} is a function of the electronic partition functions, $Q_{el}(T)$, of the reactants and the TS, σ is the rotational symmetry number, μ is the reduced mass of the reactants, $Q(T)$ is the partition function describing the translational, rotational, and vibrational degrees of freedom of the reactant, and $N^\dagger(E, J)$ is the number of states of the reactive complex for a given energy (E) and total angular momentum quantum number (J). The translational, rotational, and vibrational modes of the reaction system were assumed to be separable into sets of transitional and conserved modes.[54] The rotational partition functions were approximated by their classical limits, and the number of states of the reactive complex was calculated from the transition state theory formulation of Georgievskii and Klippenstein[34,35] using multifaceted dividing surfaces and a variable reaction coordinate (VRC-TST) considering only contributions from the transitional modes. Within VRC-TST, dividing surfaces are defined in terms of a fixed distance between pivot points on each fragment, and both the location and the separation between the pivot points are varied to determine the minimum reactive flux through a dividing surface. For the H + O_2 reaction system, the pivot points were located at each nucleus with pivot point-to-pivot point separations ranging from 3.4 to 4.5 bohr with a grid spacing of 0.1 bohr. For the H + OH reaction system, the pivot points were located at each radical orbital center with pivot point-to-pivot point separations ranging from 4.5 to 7.0 bohr with a grid spacing of 0.25 bohr. The reactive flux through a dividing surface was determined using a crude Monte Carlo sampling method[34] where the electronic structure of points on the dividing surfaces was calculated on the fly using methods described in Section 2.1.

2.3. Master Equation. The master equation (ME) for the irreversible dissociation of either HO_2 or H_2O immersed in an inert bath gas can be written as eq 5.

$$\frac{\mathrm{d}n(E,J,t)}{\mathrm{d}t} = Z\sum_{J'}\int_0^\infty P(E,J;E',J')n(E',J',t)\,\mathrm{d}E' - Zn(E,J,t) - k(E,J)n(E,J,t) \quad (5)$$

Here, $n(E, J, t)\,\mathrm{d}E$ is the number density of molecules with total energy between E and $E + \mathrm{d}E$ and with total angular momentum quantum number J at a given time t, Z is the collision rate of the molecule with the bath gas, $k(E, J)$ is the specific rate coefficient, and $P(E, J; E', J')$ is the probability of a molecule with energy between E' and $E' + \mathrm{d}E'$ and total angular momentum quantum number J' being transferred by collision to a state with energy between E and $E + \mathrm{d}E$ and total angular momentum quantum number J. The two-dimensional ME, eq 5, was reduced to an equivalent one-dimensional ME using the E, J-model of Miller et al.[55] In this model it is assumed that the J-distribution after a collision is independent of the total angular momentum of the molecule before the collision. Thus, $P(E, J; E', J') = P(E, E')\varphi(E, J)$; see Miller et al.[55] for a description of $\varphi(E, J)$. Because of the sparsity of the vibrational energy levels of the reaction systems, the vibrational density of states was computed using the method of steepest descent. The ME was solved by methods previously described[55–57] using the VARIFLEX program.[58]

The energy transfer function for deactivating collisions was modeled using the "single exponential down" expression (eq 6).

$$P(E,E') = \frac{1}{C_N(E')}\exp\left(-\frac{E'-E}{\langle\Delta E_d\rangle}\right), \quad E<E' \quad (6)$$

Here, $C_N(E')$ is a normalization constant and $\langle\Delta E_d\rangle$ is the average energy transferred by down transitions only.

The collision rate (Z) was assumed to be independent of energy and total angular momentum and was taken as the Lennard−Jones collision rate, Z_{LJ}. For the H + O_2 reaction system, the following Lennard−Jones parameters were used:[59]

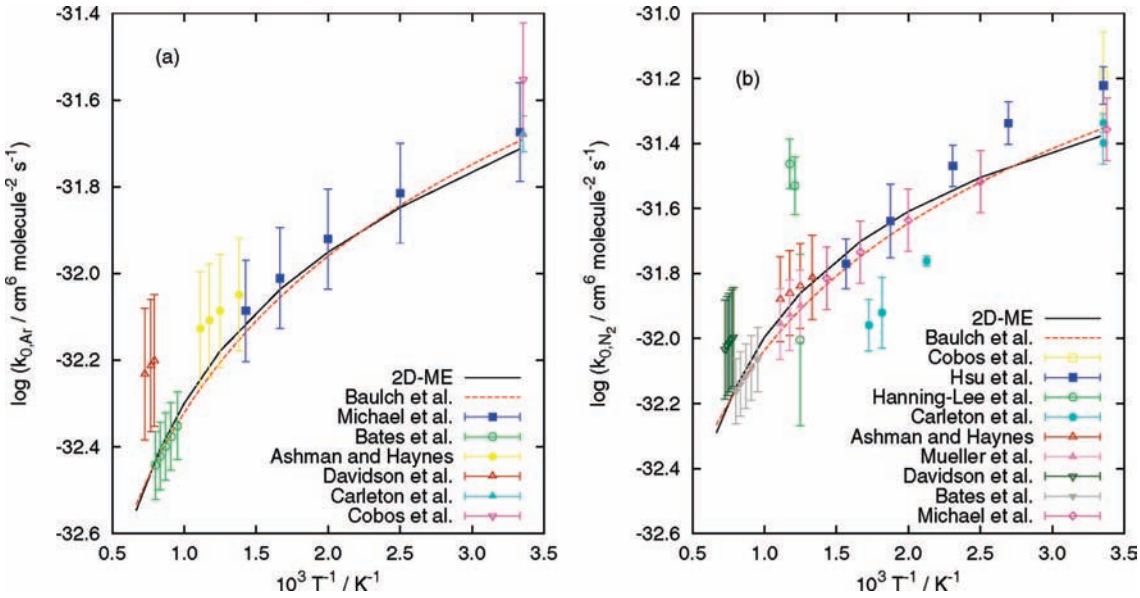

Figure 3. Low-pressure limiting rate coefficients (k_0) as a function of temperature (T) for the reactions (a) H + O_2 + Ar → HO_2 + Ar and (b) H + O_2 + N_2 → HO_2 + N_2 as calculated using a 2D-ME. References: Ashman and Haynes,[82] Bates et al.,[7] Baulch et al.,[9] Carleton et al.,[83] Cobos et al.,[6] Davidson et al.,[84] Hanning-Lee et al.,[85] Hsu et al.,[86] Michael et al.,[18] and Mueller et al.[87]

σ_{HO_2} = 3.433 Å, σ_{Ar} = 3.350 Å, σ_{N_2} = 3.652 Å, ε_{HO_2} = 254.1 cm^{-1}, ε_{Ar} = 99.5 cm^{-1}, and ε_{N_2} = 68.4 cm^{-1}, where σ is the collision diameter and ε is the well depth. For the H + OH reaction system, the following parameters were used: $\sigma_{H_2O-Ar} = 2^{-1/6}R_m$ = 3.24 Å, ε_{H_2O-Ar} = 142.98 cm^{-1}, $\sigma_{H_2O-N_2}$ = 3.43 Å, and $\varepsilon_{H_2O-N_2}$ = 441 cm^{-1} (R_m is the position of the global minimum). The parameters for the H_2O-Ar system were taken from Cohen and Saykally,[60] and the parameters for the H_2O-N_2 system were taken from Tulegenov et al.[61]

In the ME calculations, the values used for dissociation energies (at 0 K) of the $H-O_2$ and H−OH bonds were the experimental values measured by Ruscic et al.[62,63] The values used for rotational constants and vibrational frequencies of OH, O_2, H_2O, and HO_2 were experimental data taken from the NIST Computational Chemistry Comparison and Benchmark Database.[64]

3. Results

3.1. H+ O_2 (+M) → HO_2 (+M). *3.1.1. Potential Energy Surface.* Calculated equilibrium structures of the $O_2(X^3\Sigma_g^-)$ molecule and the HO_2 (X^2A'') radical are compared with experimental structures[64] in Table S1 (Supporting Information). Bond lengths and bond angles obtained with the CASPT2 model are in good agreement with parameters obtained with the MP2 and B3LYP models, and all results are within expected error margins.[38,65]

Table 1 gives electronic (D_e) and bond (D_0) dissociation energies (at 0 K) of the $H-O_2$ bond as calculated at several levels of theory. As can be seen, the B3LYP/aug-cc-pVTZ model and the five different CCSD(T) calculations are in excellent agreement with the experimental value of 47.99 ± 0.06 kcal mol^{-1},[63] taking into account that the zero-point vibrational energies have been calculated within the harmonic oscillator approximation. If the anharmonic ZPE is included, D_0 = 48.4 kcal mol^{-1} at the CCSD(T)/EB5Q//MP2/aug-cc-pVTZ level of theory. Compared to the CCSD(T)/EB5Q//MP2/aug-cc-pVTZ level of theory, the CASPT2/aug-cc-pVTZ model underestimates D_e by 10.9 kcal mol^{-1}. The CASPT3/aug-cc-pVTZ//CASPT2/aug-cc-pVTZ model, on the other hand, overestimates D_e by 7.5 kcal mol^{-1}. Harding et al.[10]predicted a bond dissociation energy of 44.4 kcal mol^{-1} at the CAS+1+2+QC/aug-cc-pVTZ level of theory.

Figure 1 shows the minimum energy path (MEP) for reaction 1 as a function of the $H-O_2$ bond length, r_{H-OO} , as calculated at the CASPT2/aug-cc-pVTZ level with relaxed and constrained optimization of the HO−O bond length, r_{HO-O}. The effect of basis set size is shown in Table S2 (Supporting Information). As can be seen, the aug-cc-pVTZ basis gives a sufficiently accurate description of the reaction system compared to the larger aug-cc-pVQZ basis; the aug-cc-pVDZ basis is too small. The effect of inclusion of zero-point vibrational energy along the MEP was investigated at the B3LYP/aug-cc-pVTZ level of theory, see Table S3 (Supporting Information). Note, however, that only the contribution from the HO−O stretching mode is included in the ZPE because this mode is assumed to be "conserved" during the reaction. The electronic energy along the MEP as calculated with r_{HO-O} constrained at the equilibrium value of the O_2 molecule is of similar magnitude as the energy with ZPE included and relaxed r_{HO-O} bond length for $r_{H-OO} >$ 2 Å. At large separation of the fragments it is therefore reasonable to assume that the contribution from the conserved O−O stretching mode cancels.[66,67] This approximation becomes worse when $r_{H-OO} <$ 2 Å.

The result of Harding et al.[10] obtained with the CAS+1+2+QC/aug-cc-pVTZ model is included in Figure 1 for comparison. As can be seen, the CASPT2 model and the model employed by Harding and co-workers give nearly identical results for $r_{H-OO} >$ 2.8 Å; however, the CAS+1+2+QC model predicted a much more attractive potential at shorter distances than the CASPT2 model employed in this work. The CAS+1+2 calculations of Harding et al. were carried out using the COLUMBUS program.[68]

To investigate this issue more thoroughly, additional calculations were carried out using the CAS+1+2 and CAS+1+2+QC models implemented in MOLPRO and the multireference MP2 (MRMP2) model of Hirao [69,70] implemented in GAMESS.[47,48] The aug-cc-pVTZ basis set was employed in all calculations. The results from these calculations are included in Figure 1. As can be seen, the CAS+1+2 model predicted a Born−Oppenheimer barrier to reaction of about 0.1 kcal mol^{-1} relative to the energy

of the reactants, which obviously is not correct. The situation improved when the Davidson correction was included, but still, the calculation predicted a small barrier to reaction below the energy of the reactants. The CAS+1+2 and CAS+1+2+QC models employed in this work differ from the CASPT2 model and the model used by Harding et al.[10] at longer r_{H-OO} distances too, predicting less attractive potential. The CASPT2 and MRMP2 models give nearly identical results at $r_{H-OO} > 2.8$ Å, but the MRMP2 model predicts a slightly less attractive potential in the region $2.3 < r_{H-OO} < 2.8$ Å and predicts a significantly more attractive potential when $r_{H-OO} < 2.3$ Å. The B3LYP and MRMP2 models predict similar results when $r_{H-OO} < 2$ Å, but the B3LYP model fails at longer distances, which is expected.

3.1.2. High-Pressure Limiting Rate Coefficient. Figure S1 (Supporting Information) shows the part of the X^2A'' potential energy hypersurface of reaction 1 sampled in the VRC-TST calculation of the high-pressure limiting rate coefficient. Each scatter point represents a single-point energy calculation at the CASPT2/aug-cc-pVTZ level of theory. Taking $f_{el} = Q_{el}(HO_2)/Q_{el}(H)Q_{el}(O_2) = 1/3$, the following expression for $k_{1,\infty}$ was extracted over the temperature range 300−3000 K.

$$k_{1,\infty}(T) = (25T^{-0.367} + 7.5\times10^{-2}T^{0.702})\times 10^{-11}\ \mathrm{cm^3\ molecule^{-1}\ s^{-1}} \quad (7)$$

The high-pressure limiting rate coefficient of reaction 1 calculated in this work is compared with previous experimental[6,7] and theoretical[10,12,32,71] results in Figure 2. As can be seen, our calculated $k_{1,\infty}$ is roughly 25% lower than that calculated by Harding et al.[10] or by Marques and Varandas.[12,71] On the other hand, our result is in very good agreement with the experimental value at 298 K reported by Cobos et al.[6] Recently, Troe[11] investigated the falloff behavior of reaction 1 and found that the center broadening factor (F_{cent}) remained nearly unchanged from the value used in the study from 1985.[6] Therefore, the experimental value of $k_{1,\infty}(298\ \mathrm{K}) \approx 7.5\times10^{-11}$ cm^3 molecule^{-1} s^{-1} also remains nearly unchanged. Troe[11] argued, however, that neglect of the onset of diffusional effects at pressures above 10 bar may lead to an underestimation of the experimental $k_{1,\infty}$ by as much as 10−20%. Still, we find the agreement between this work and the experimental value of Cobos and co-workers[6] to be satisfactory. The high-pressure limiting rate coefficient reported by Bates et al.,[7] based on RRKM analysis of experimental data obtained at temperatures between 1050 and 1250 K, is significantly lower than predicted by any of the theoretical studies. We note, however, that the reaction rates measured by Bates and colleagues just enter the falloff regime at the highest pressures investigated. Because of this, together with the use of a rather simple Hindered-Gorin model, their fitted high-pressure limiting rate coefficient is likely affected by a rather larger uncertainty. We have no reason to believe, however, that the experimental data of Bates et al.[7] are affected by large errors.

3.1.3. Pressure Dependence. Figure 3, panels a and b, shows calculated low-pressure limiting rate coefficients over the temperature range 300−1500 K for reaction 2 with Ar and N_2 as bath gases, respectively. As can be seen, the values calculated with the two-dimensional ME (2D-ME) are in good agreement with both the experimental values and the IUPAC evaluation[9] over the whole temperature range investigated. Over the temperature range 300−3000 K, the calculated low-pressure limiting rate coefficients could be fitted to the following expressions.

$$k_0(H + O_2 + Ar) = 9.1\times 10^{-29}T^{-1.404}\exp(-134/T)\ \mathrm{cm^6\ molecule^{-2}\ s^{-1}} \quad (8)$$

$$k_0(H + O_2 + N_2) = 2.0\times 10^{-27}T^{-1.73}\exp(-270/T)\ \mathrm{cm^6\ molecule^{-2}\ s^{-1}} \quad (9)$$

For comparison, the values preferred by the IUPAC panel are $k_0 = 1.9\times10^{-29}T^{-1.2}$ cm^6 molecule^{-2} s^{-1} for Ar as bath gas and $k_0 = 7.3\times10^{-29}T^{-1.3}$ cm^6 molecule^{-2} s^{-1} for N_2 as bath gas.[9]

Calculated falloff curves for reaction 1 at 300 K with Ar and N_2 as bath gases are shown in Figure 4, panels a and b, respectively. Similar falloff curves at 800 and 1250 K are shown in Figure S2 (Supporting Information). Again, there is good agreement between our calculated values and the experimental values over the whole temperature and pressure range for which experimental data are available. Especially, there is very good agreement between our values and the values measured by Bates et al.,[7] Hahn et al.,[8] and Michael el al.[18] The 1D-ME significantly overestimates the reaction rate coefficient except at very high pressures.

The falloff curves were obtained using $\langle\Delta E_d\rangle = 45(T/298\ \mathrm{K})^{0.95}$ cm^{-1} and $\langle\Delta E_d\rangle = 100(T/298\ \mathrm{K})^{0.65}$ cm^{-1} for Ar and N_2

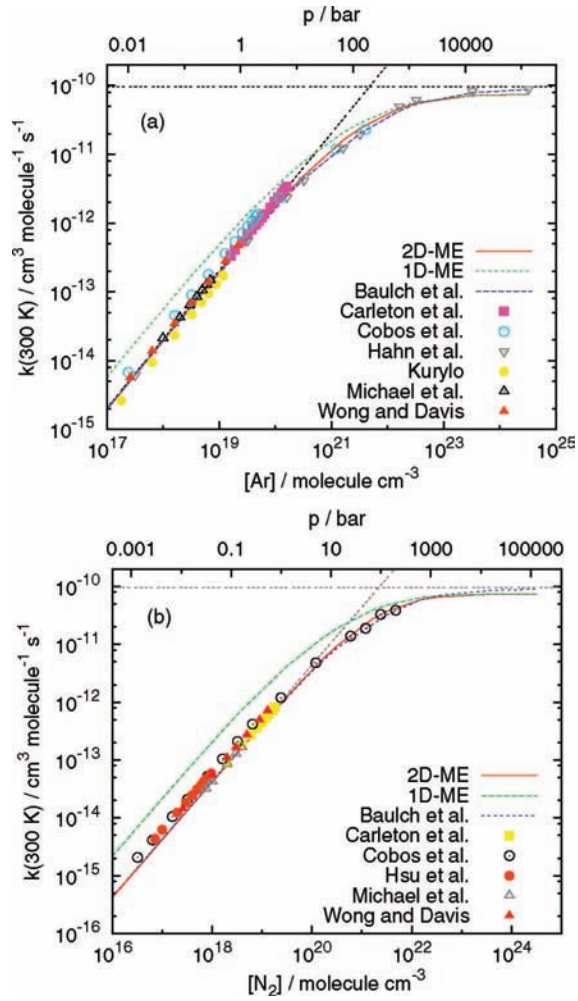

Figure 4. Falloff curves for the reactions (a) $H + O_2 + Ar \rightarrow HO_2 + Ar$ and (b) $H + O_2 + N_2 \rightarrow HO_2 + N_2$ at 300 K as calculated using 1D-ME and 2D-ME. The plotted low-pressure and high-pressure limiting rate coefficients are the values preferred by the IUPAC panel.[9] References: Baulch et al.,[9] Carleton et al.,[83] Cobos et al.,[6] Hahn et al.,[8] Hsu et al.,[86] Kurylo,[88] Michael et al.,[18] and Wong and Davis.[89]

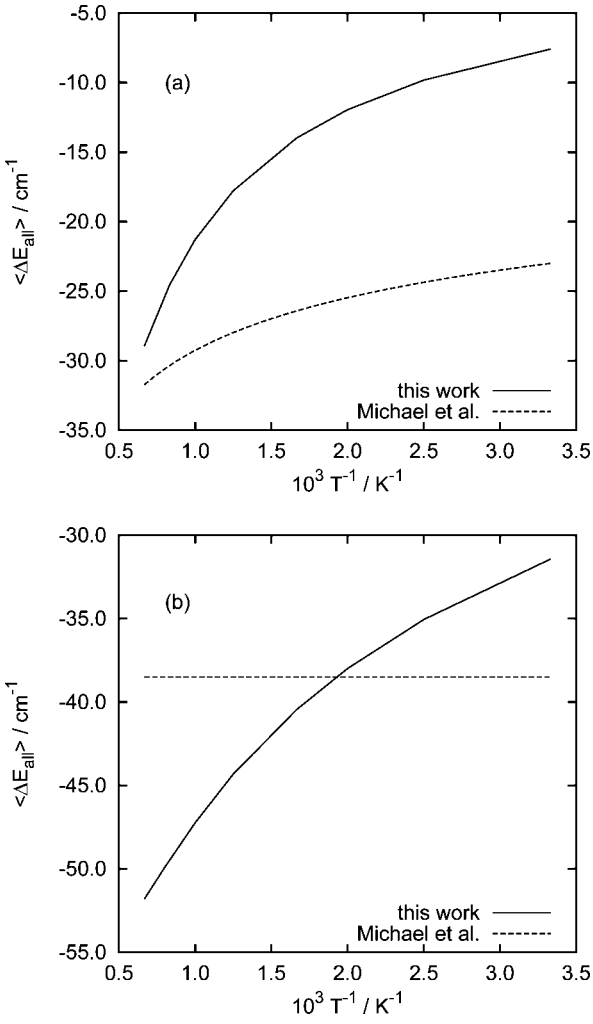

Figure 5. Values of $\langle\Delta E_{all}\rangle$ for the reactions (a) H + O_2 + Ar → HO_2 + Ar and (b) H + O_2 + N_2 → HO_2 + N_2 as deduced from a two-dimensional master equation (this work) and the experimental study of Michael et al.[18]

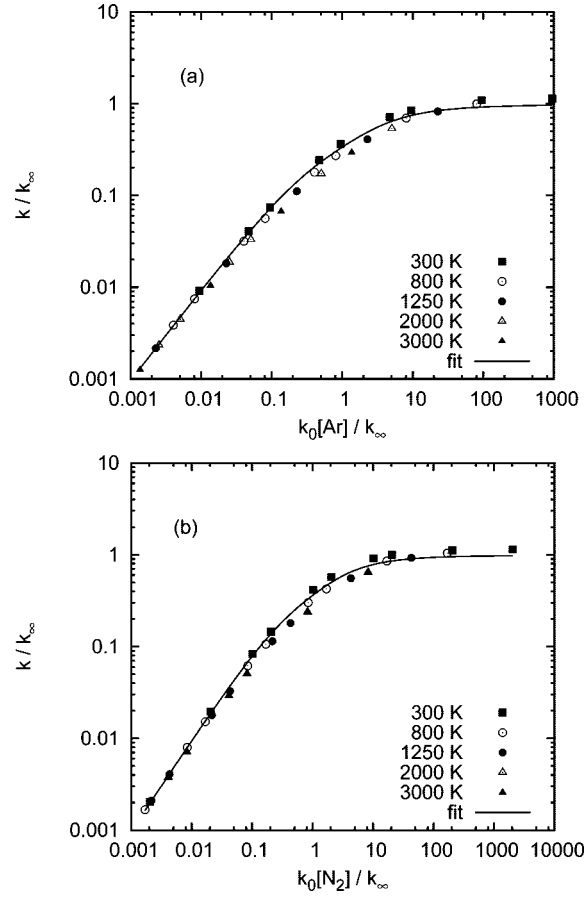

Figure 6. Doubly reduced falloff curve for the reactions (a) H + O_2 + Ar → HO_2 + Ar and (b) H + O_2 + N_2 → HO_2 + N_2 as calculated using a two-dimensional master equation (scatter points). Fit of the data to eq 10 gave a center broadening factor of $F_{cent} = 0.67 \pm 0.03$ for Ar as bath gas and $F_{cent} = 0.72 \pm 0.03$ for N_2 as bath gas (the error corresponds to 1σ from the statistical analysis).

as bath gases, respectively. The average energies transferred by all transitions, $\langle\Delta E_{all}\rangle$, for the reactions H + O_2 + Ar and H + O_2 + N_2 are plotted in Figure 6, panels a and b, respectively. As can be seen, the values for $\langle\Delta E_{all}\rangle$ deduced from the 2D-ME are quite different from the values deduced from the experimental study by Michael et al.[18] $\langle\Delta E_{all}\rangle$ for the H + O_2 + Ar reaction reported by Teitelbaum et al.[17] has not been included in Figure 6a. In the study by Teitelbaum and co-workers, $\langle\Delta E_{all}\rangle$ varied from -376 cm^{-1} at 300 K to -98 cm^{-1} at 8000 K.

Doubly reduced falloff curves for reaction 1 with Ar and N_2 as bath gases are displayed in Figure 5, panels a and b, respectively. The falloff behavior could be described by the following symmetric expression,[72]

$$\frac{k}{k_\infty} = \left(\frac{x}{1+x}\right) F_{cent}^{1/\,[1+(\log x/N)^2]} \qquad (10)$$

where $x = k_0[M]/k_\infty$, $N \approx 0.75-1.27 \log F_{cent}$, and F_{cent} is the center broadening factor. Under the assumption that F_{cent} is independent of temperature, fit of the data in Figure 5, panels a and b, to eq 10, gave $F_{cent} = 0.67 \pm 0.03$ for Ar as bath gas and $F_{cent} = 0.72 \pm 0.03$ for N_2 as bath gas over the temperature range 300−3000 K (1σ). This is in contrast to the center broadening factors reported by the IUPAC panel[9] and Troe.[11] The IUPAC panel[9] reported $F_{cent} = 0.51 \pm 0.1$ and $F_{cent} = 0.57 \pm 0.1$ for Ar and N_2 as bath gases, respectively. The center broadening factors reported by Troe[11] were essentially identical to the values reported by the IUPAC panel.

3.2. H + OH (+M) → H_2O (+M). *3.2.1. Potential Energy Surface.* Calculated equilibrium structures of OH($X^2\Pi$) and $H_2O(X^1A_1)$ are in good agreement with experimental structures,[64] see Table S1 (Supporting Information). In Table 2 the dissociation energy of the H−OH bond as calculated at several levels of theory is compared with the experimental value of 117.59 ± 0.07 kcal mol^{-1} determined by Ruscic et al.[62] As can be seen, the bond dissociation energy obtained at the CCSD(T)/EB5Q//MP2/aug-cc-pVTZ level of theory with anharmonic ZPE included is only 0.4 kcal mol^{-1} higher than the experimental value. At the CASPT2/aug-cc-pVTZ level of theory, D_e and D_0 are underestimated by 2.6 and 2.9 kcal mol^{-1}, respectively, relative to the CCSD(T)/EB5Q//MP2/aug-cc-pVTZ level of theory. Inclusion of higher-order excitations improved the situation; the discrepancy between the CASPT3/EBQT//CASPT2/aug-cc-pVTZ and CCSD(T)/EB5Q//MP2/aug-cc-pVTZ models is ∼1.5 kcal mol^{-1}.

Figure 7 displays the MEP for reaction 2 as a function of the H−OH′ bond length ($r_{H-OH'}$) calculated at the CASPT2/aug-cc-pVTZ and UB3LYP/aug-cc-pVTZ levels of theory with relaxed and constrained optimization of the HO−H′ bond length. The CASPT2 model predicted a significantly more attractive potential than the B3LYP model in the important region $2 < r_{H-OH'} < 4$ Å. The effect of expansion of the basis set was

TABLE 2: Electronic (D_e) and Bond (D_0) Dissociation Energies (at 0 K) of the H−OH Bond of $H_2O(X^1A_1)$

method[a]	D_e/kcal mol^{-1}	D_0/kcal mol^{-1} harmonic	D_0/kcal mol^{-1} anharmonic
B3LYP/aTZ	122.6	114.5	
MP2/aTZ	127.3	119.3	119.6
CCSD(T)/aTZ//MP2/aTZ	123.6	115.6	115.9
CCSD(T)/aQZ//MP2/aTZ	125.0	116.9	117.3
CCSD(T)/a5Z//MP2/aTZ	125.3	117.3	117.6
CCSD(T)/EBQT//MP2/aTZ	126.0	118.0	118.3
CCSD(T)/EB5Q//MP2/aTZ	125.6	117.6	118.0
CASPT2/aTZ	123.0	114.7	
CASPT3/aTZ/CASPT2/aTZ	122.1	113.9	
CASPT3/aQZ/CASPT2/aTZ	123.4	115.2	
CASPT3/EBQT/CASPT2/aTZ	124.3	116.1	
CAS+1+2+QC/aug-cc-pVTZ[b]	123.8		
experiment[c]	125.8		
experiment[d]			117.59 ± 0.07

[a] Abbreviations: a*XZ* = aug-cc-pV*XZ*; EB*XY* = basis set extrapolation of aug-cc-pV*XZ* and aug-cc-pV*YZ* where $Y = X - 1$; see eq 3. [b] See Ho et al.[29] [c] Based on $\Delta_f H$ (0 K) values; see Table I in Ho et al.[29] for details. [d] See Ruscic et al.[62]

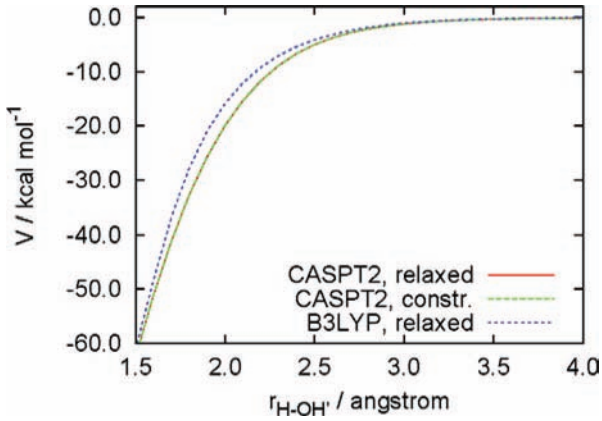

Figure 7. Minimum energy path for the reaction H + OH → H_2O (X^1A') as a function of $r_{H-OH'}$, as calculated using the CASPT2 and B3LYP models employing the aug-cc-pVTZ basis set with relaxed and constrained $r_{HO-H'}$. The energies are relative to the energy of the reactants and include electronic energy only.

investigated for the CASPT2 model; see Table S4 (Supporting Information). Again, the aug-cc-pVTZ basis provided a sufficiently accurate description of the MEP compared to the larger aug-cc-pVQZ basis. Table S5 (Supporting Information) shows the effect of inclusion of ZPE along the MEP as investigated at the UB3LYP/aug-cc-pVTZ level of theory. Only the contribution from the "conserved" O−H stretching mode was included in the ZPE. As can be seen, the contribution from the conserved O−H stretching mode nearly cancels over the whole region investigated.

The effect of spin−orbit (SO) coupling along the minimum energy path for reaction 2 was also investigated. The MEP was calculated at the CASPT2/aug-cc-pVTZ level of theory, whereas the SO matrix elements were computed using the Breit−Pauli Hamiltonian. Wavefunctions for the SO states were generated using MRCI with CASSCF reference configurations only and the 6-311++G(3df,p) basis set. At infinite separation of the H(^{2}S) + OH($X^2\Pi$) fragments, the four ground-state potential energy hypersurfaces of the system converge to two doubly-degenerate surfaces separated by the SO coupling constant. In the asymptotic region of the reactants, the calculated SO coupling constant, 136.5 cm^{-1} , agrees well with the experimental value, 138.68 ± 0.02 cm^{-1}.[73] When $r_{H-OH'}$ < 4.5 Å, the four SO states start to significantly split and only one PES correlate with $H_2O(X^1A_1)$; see Figure S3 (Supporting Information).

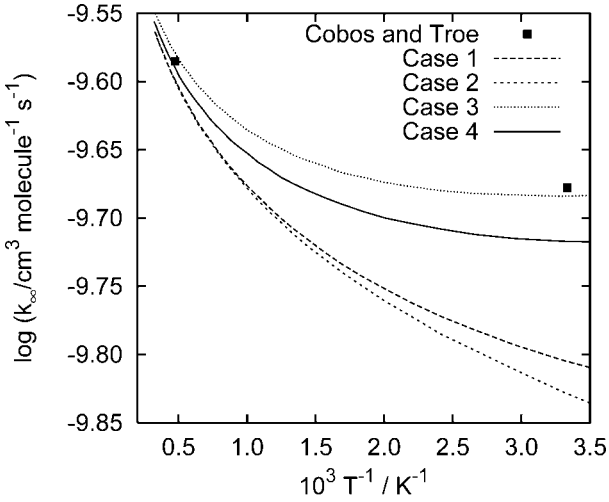

Figure 8. High-pressure limiting rate coefficient (k_∞) as a function of temperature (T) for the reaction H + OH → H_2O (X^1A'). See Section 3.2.2 for a description of cases 1–4. References: Cobos and Troe.[32]

3.2.2. High-Pressure Limiting Rate Coefficient. The part of the X^1A' potential energy hypersurface sampled in the VRC-TST calculation of $k_{2,\infty}$ is shown in Figure S4 (Supporting Information). The PES was obtained at the CASPT2/aug-cc-pVTZ level of theory.

The effect of spin−orbit coupling on the high-pressure limiting rate coefficient was investigated in four different ways. In case 1, no SOC was included and f_{el} was taken as eq 11.

$$f_{el} = \frac{Q_{el}(H_2O)}{Q_{el}(H)Q_{el}(OH)} = \frac{1}{8} \quad (11)$$

In case 2, SOC was included in the asymptotic region of the reactants, and f_{el} was taken as eq 12,

$$f_{el} = \frac{1}{4[\exp(E_{SO}/2k_BT) + \exp(-E_{SO}/2k_BT)]} \quad (12)$$

where E_{SO} = 138.68 cm^{-1} is the energy splitting between the SO states. In case 3, the asymptotic potential energy of the reactants was shifted to the lowest SO state, and f_{el} was taken as eq 13.

$$f_{el} = \frac{1}{4[1 + \exp(-E_{SO}/k_BT)]} \quad (13)$$

Finally, in case 4 SO coupling was explicitly included by calculating the potential energy relative to the lowest spin−orbit state over the whole surface sampled using the same procedure as used in Section 3.2.1. Again, eq 13 was used for f_{el}.

The results obtained for the four different cases are shown in Figure 8. For the case where spin−orbit coupling was treated explicitly, the following expression for $k_{2,\infty}$ was obtained over the temperature range 300−3000 K.

$$k_{2,\infty}(T) = 4.17 \times 10^{-11} T^{0.234} \exp(57.5/T) \text{ cm}^3 \text{ molecule}^{-1} \text{ s}^{-1} \quad (14)$$

There is a significant difference between the case where no SO coupling was included and the case where SO coupling was explicitly treated. Further, if spin−orbit coupling is not explicitly treated, care should be exercised on how f_{el} is treated. Shifting the asymptotic potential energy of the reactants to the lowest

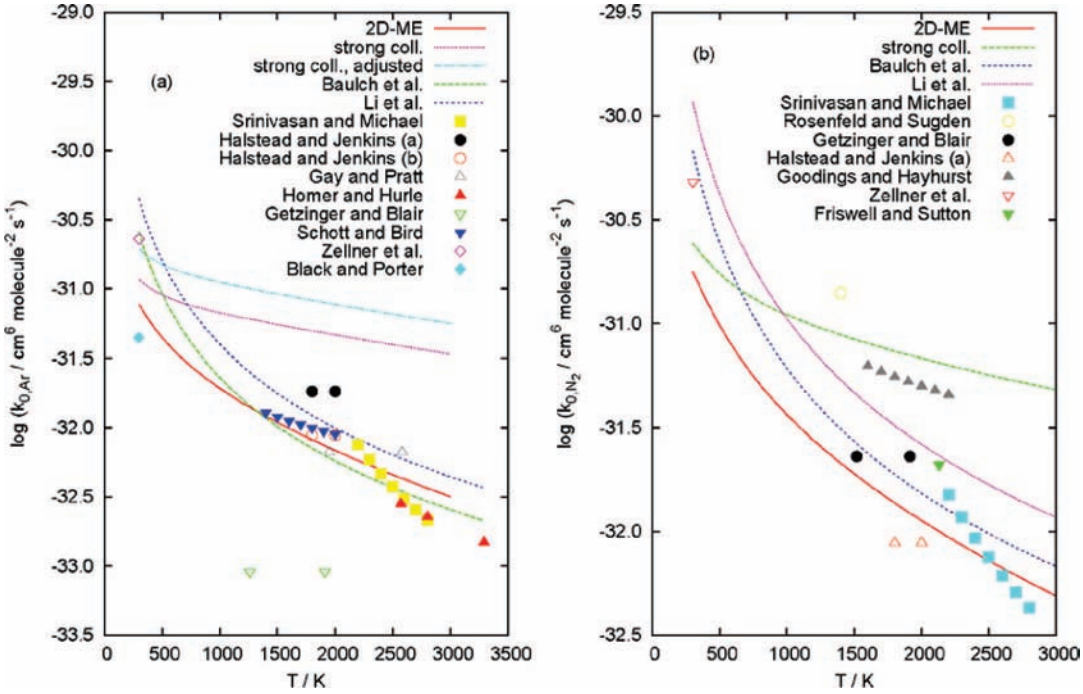

Figure 9. Low-pressure limiting rate coefficients (k_0) as a function of temperature (T) for the reactions (a) H + OH + Ar → H_2O + Ar and (b) H + OH + N_2 → H_2O + N_2 as calculated using 2D-ME, strong collision RRKM analysis (strong coll.), and strong collision RRKM analysis with adjusted Lennard−Jones parameters (strong coll., adjusted); see text for details. References: Baulch et al.,[9] Black and Porter,[79] Friswell and Sutton,[90] Gay and Pratt,[91] Getzinger and Blair,[92] Goodings and Hayhurst,[93] Halstead and Jenkins (a),[94] Halstead and Jenkins (b),[95] Homer and Hurle,[96] Li et al.,[2] Rosenfeld and Sugden,[97] Schott and Bird,[98] Srinivasan and Michael,[27] and Zellner et al.[78]

spin−orbit state and using eq 12 for f_{el} provides a good approximation to the case with SO coupling explicitly treated; the second case with f_{el} given according to eq 11 does not. In Figure 8, one also observes that the simplified statistical adiabatic channel model used by Cobos and Troe[32] performs remarkably well compared to the results obtained in this work.

3.2.3. Pressure Dependence. Figure 9, panels a and b, shows calculated and experimental low-pressure limiting rate coefficients for reaction 2 with Ar and N_2 as bath gases, respectively. The calculated low-pressure limiting rate coefficients were obtained using a 2D-ME, eq 5, where the value of $\langle \Delta E_d \rangle$ was adjusted to give best possible agreement with the experimental data. The expressions $300(T/298\ \mathrm{K})^{0.5}\ \mathrm{cm}^{-1}$ and $400(T/298\ \mathrm{K})^{0.4}\ \mathrm{cm}^{-1}$ were used for $\langle \Delta E_d \rangle$ for reaction 2 with Ar and N_2 as bath gases, respectively. Over the temperature range 300−3000 K, the calculated low-pressure limiting rate coefficients could be fitted to the following expressions:

$$k_0(\mathrm{H+OH+Ar}) = 8.6\times 10^{-28} T^{-1.527} \exp(-185/T)\ \mathrm{cm}^6\ \mathrm{molecule}^{-2}\ \mathrm{s}^{-1} \quad (15)$$

$$k_0(\mathrm{H+OH+N_2}) = 1.25\times 10^{-26} T^{-1.81} \exp(-251/T)\ \mathrm{cm}^6\ \mathrm{molecule}^{-2}\ \mathrm{s}^{-1} \quad (16)$$

Figure 10, panels a and b, shows doubly reduced falloff curves for reaction 2 with Ar and N_2 as bath gases, respectively. Fit of the data to eq 10 gave the following center broadening factors: $F_{cent} = 0.72 \pm 0.01$ for Ar as bath gas and $F_{cent} = 0.73 \pm 0.01$ for N_2 as bath gas (1σ).

For comparison, the low-pressure limiting rate coefficients preferred by the IUPAC panel[9] are $k_0(\mathrm{H+OH+Ar}) = 2.3\times10^{-26}T^{-2.0}\ \mathrm{cm}^6\ \mathrm{molecule}^{-1}\ \mathrm{s}^{-1}$ and $k_0(\mathrm{H+OH+N_2}) = 6.1\times10^{-26}T^{-2.0}\ \mathrm{cm}^6\ \mathrm{molecule}^{-1}\ \mathrm{s}^{-1}$ over the temperature range 300−3000 K. As can be seen from Figure 9, panels a and b, our calculated low-pressure limiting rate coefficient when Ar is bath gas is slightly larger than the IUPAC preferred value when the temperature is larger than 1500 K but is more than a factor of 3 lower at 300 K. When N_2 is bath gas, there again is

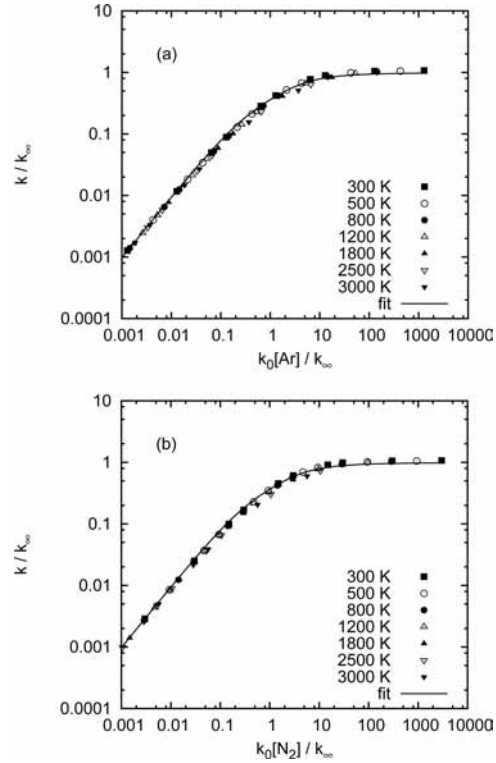

Figure 10. Doubly reduced falloff curve for the reactions (a) H + OH + Ar → H_2O + Ar and (b) H + OH + N_2 → H_2O + N_2 as calculated using a 2D-ME (scatter points). Fit of the data to eq 10 gave a center broadening factor of $F_{cent} = 0.72 \pm 0.01$ for Ar as bath gas and $F_{cent} = 0.73 \pm 0.01$ for N_2 as bath gas (the error corresponds to 1σ from the statistical analysis).

modest agreement between our calculated k_0 and the IUPAC preferred k_0 when the temperature is larger than 1000 K and is different by more than a factor of 3 at 300 K.

Srinivasan and Michael[27] have recently studied the thermal decomposition of water. Using a reflected shock tube technique, they measured $k_0(H_2O + Ar) = (2.43 \pm 0.57)\times10^{-10}\exp(-(47117 \pm 633)/T)$ cm^3 molecule^{-1} s^{-1} over the temperature range 2196−3290 K. Taking $K_{eq} = 2.209\times10^{24}T^{0.1879}\exp(-59608.8/T)$ molecules cm^{-3} as the equilibrium coefficient,[27] one gets $k_0(H + OH + Ar) = 1.1\times10^{-34}T^{-0.1879}\exp(12491.8/T)$ cm^6 molecule^{-2} s^{-1}. We can see in Figure 9, panels a and b, that our low-pressure limiting rate coefficients calculated using a 2D-ME cannot fully reproduce the temperature dependence of reaction 2 measured by Srinivasan and Michael,[27] neither when Ar nor N_2 is bath gas.

4. Discussion

The potential energy hypersurfaces involved in reactions 1 and 2 have been studied using several ab initio methods and basis sets. The apparent difference between the CAS+1+2/CAS+1+2+QC calculations of this work on the H + O_2 reaction system and the work of Harding et al.[10] is disturbing considering the same active space was used in the two calculations. Possibly, it is related to the different implementations of MRCI in the program packages MOLPRO (used in this work)[41] and COLUMBUS (used by Harding et al.),[68] the former program using an internal contraction scheme. Celani et al.[74] found that the dissociation energy of Cr_2 obtained from an uncontracted MRCI calculation performed with the COLUMBUS program was about 0.09 eV larger than the dissociation energy obtained with the internally contracted MRCI (MOLPRO). Abrams and Sherrill[75] have also suggested that the MRCI approach is somewhat more sensitive to the choice of active space than the CASPT2 model. Klippenstein et al.[76] have investigated the reaction $CH_3 + CH_3$ and related reactions at the CASPT2/aug-cc-pVTZ and CAS+1+2+QC/aug-cc-pVTZ levels of theory. With increasing active space, they found the CASPT2 model to be more accurate along the reaction path, but the CAS+1+2+QC model may be more accurate away from the reaction path. It should be noted, however, that the calculations of Klippenstein and co-workers were carried out with the MOLPRO[41] package. We have therefore chosen to use the CASPT2 method to obtain potential energy hypersurfaces needed for the VRC-TST calculations, because the CASPT2 method does not give the same artifacts as the CAS+1+2+QC method for the H + O_2 reaction system, and it is computationally less expensive than the CASPT3 method.

As mentioned in Section 3.1.2, the high-pressure limiting rate coefficient for reaction 1 calculated in this work is about 25% lower than obtained by Harding et al.[10] or by Marques and Varandas.[12,71] This discrepancy can be attributed to differences in the potential energy hypersurface of the reaction predicted by the different studies. Our calculation at the CASPT2/aug-cc-pVTZ level of theory predicted a less attractive potential than the CAS+1+2+QC/aug-cc-pVTZ potential used by Harding et al. or the DMBE IV potential[15] used by Marques and Varandas, see Figure 1. It is important to mention here that Klippenstein and co-workers[76] have found that the VRC-TST approach overestimates the capture rate for the $CH_3 + CH_3$ reaction system by 10−20% compared to classical trajectory calculations. Our preliminary calculations suggest that this is also the case for the OH + OH → H_2O_2 reaction. Most likely, this also applies to the reaction systems studied in this work. The effect of the less attractive PES obtained in this work, may thus be countered to some extent by the overestimation of the capture rate by the VRC-TST model.

In the ME analysis of the H + OH + N_2 reaction we have used Lennard−Jones (LJ) parameters of a hydrogen-bonded $H_2O\cdots N_2$ complex.[61] However, another alternative is to use LJ parameters of a T-shaped $H_2O\cdots N_2$ complex.[77] For completeness, Figure S5 (Supporting Information) shows a comparison of $k_0(T)$ obtained from 2D-ME calculations using the two different sets of LJ parameters. The same expression for $\langle\Delta E_d\rangle$, $400(T/298\text{ K})^{0.4}$ cm^{-1}, was used in the two cases. As can be seen in Figure S5, $k_0(T)$ for the case with LJ parameters of a T-shaped complex is significantly lower than for the case with LJ parameters of a H-bonded complex at all temperatures. To get better agreement between the two cases, larger values for $\langle\Delta E_d\rangle$ are needed when using LJ parameters of the T-shaped complex. In any case, the interaction between H_2O and N_2 is not correctly described by a LJ potential. However, it has become common practice to define a collision in terms of the LJ collision rate.[57] Thus, the reported values for $\langle\Delta E_d\rangle$ should be interpreted in light of the LJ parameters used.

We see in Figure 9, panels a and b, that there are large discrepancies between our values for $k_{2,0}$ at 300 K and the values measured by Zellner et al.[78] and by Black and Porter.[79] We note it is possible to get agreement with the Black and Porter results by lowering the value used for $\langle\Delta E_d\rangle$. However, this will deteriorate the agreement with the results of Srinivasan and Michael[27] at higher temperatures, which we consider to be more reliable results. An important question to be answered, therefore, is why there is such a large discrepancy between our calculations and the measurements by Zellner and colleagues. In the following we will investigate this issue more thoroughly.

Included in Figure 9a is a plot of $k_0(H + OH + Ar)$ as calculated from a strong-collision RRKM analysis using the same LJ parameters and $D_0(H-OH)$ as used in the 2D-ME analysis. As can be seen, the value of $k_0(300\text{ K})$ increases, but not enough to explain the value measured by Zellner et al.[78] In fact, it was necessary to increase the LJ collision diameter of H_2O to 5 Å in order to explain the rate coefficient at 300 K measured by Zellner et al.[78] Clearly, the assumptions of strong collisions and $\sigma_{H_2O} = 5$ Å are unreasonable.

We have assumed that the termolecular association reactions take place via an energy-transfer mechanism. One could speculate whether the discrepancy between this work and the work of Zellner et al.[78] is due to contribution from the so-called chaperon mechanism. To our knowledge, there is no information about the importance of the chaperon mechanism for reaction 2. However, Marques et al.[80] have investigated the chaperon mechanism for the H + O_2 + Ar reaction. In Figure 11 in the paper of Marques et al.,[80] we see the reactive cross-section for HO_2 formation significantly drops when the translational energy increases from 0.25 to 2.0 kcal mol^{-1}. Similarly, Rodrigues and Varandas[81] found that the energy transfer mechanism and the chaperon mechanism for the H + CN + Ar reaction are only competitive at low temperatures. Therefore, it is likely that the chaperon mechanism is of minor importance for the H + OH + Ar reaction also. The interaction between H_2O and N_2 is stronger than between H_2O and Ar.[60,61] Thus, the chaperon mechanism could be of greater importance for reaction 2 when nitrogen is bath gas. Still, it is questionable that the contribution from the chaperon mechanism can explain the factor of 3 difference between this work and the work of Zellner et al.[78] for the H + OH + N_2 reaction at 300 K, given that there is a large discrepancy when argon is bath gas also. In any case, the

chaperon mechanism will be of minor importance at temperatures relevant for combustion.

The ME calculations presented in this work neglect effects of anharmonic vibrations. One could therefore argue that this might make up some of the difference between this study and the work of Zellner et al.[78] In the low-pressure limit, anharmonicity impacts the rate coefficient through the density of states near the dissociation limit and the effect should not depend very much on the temperature. Given the good agreement between our ME calculations and the experimental data for the $H + O_2$ reaction system, we do not believe that the discrepancy between this work and the work of Zellner and co-workers can be explained by the neglect of anharmonic effects only. However, it cannot be ruled out and it is likely that anharmonic effects will be of some importance for the $H + OH$ reaction.

In the kinetic models of both Li et al.[2] and Ó Conaire et al.[3] it was necessary to increase the *A* factor of reaction 2 by a factor of two compared to the preferred value of the IUPAC panel in order to explain observed laminar flame speeds. Li et al.[2] noted that because of the large uncertainty in the rate coefficient of reaction 2, laminar flame speed predictions using any particular set of recommended diffusion coefficients can be forced to predict the same laminar flame speed by adjusting the value of this rate coefficient. On the basis of our calculations, such an increase in the rate coefficient is not warranted at temperatures below 1000 K. For higher temperatures we cannot completely rule out that the rate coefficient can be a factor of 2 larger. However, both our study and the experimental study by Srinivasan and Michael[27] indicate that $k_{2,0}$ should be lower than the value used by Li et al.[2] and Ó Conaire et al.[3] at higher temperatures, at least for temperatures above 2000 K. We agree, however, with the comment by Srinivasan and Michael[27] that the apparent rate coefficient at high temperatures might be higher depending on the extent of reaction etc. in the various flame regions.

Conclusions

Potential energy hypersurfaces of the reactions $H + O_2$ (+M) $\rightarrow HO_2$ (+M) and $H + OH$ (+M) $\rightarrow H_2O$ (+M) have been investigated using high-level quantum chemistry methods. High-pressure limiting rate coefficients obtained using variable reaction coordinate transition state theory are reported. For the first time, the pressure dependence of the reactions has been investigated using a 2D-ME. Our calculations on the $H + O_2$ reaction system with Ar and N_2 as bath gases can explain the experimental data at all temperatures and pressures investigated. The ME calculations on the $H + OH$ reaction with Ar and N_2 as bath gases can describe reasonably well the experimental high-temperature data of Srinivasan and Michael,[27] but it cannot explain the low-pressure limiting rate coefficients measured by Zellner et al.[78] at 300 K without making unrealistic assumptions. New measurements at room temperature of the low-pressure limiting rate coefficient would be of value in order to provide a better description of the $H + OH$ (+M) $\rightarrow H_2O$ (+M) reaction.

Acknowledgment. This work was supported by the Research Council of Norway under Contract No. 173826/I30. The Norwegian Metacenter for Computational Science (NOTUR) is acknowledged for grants of computing time. Sandia is a multiprogram laboratory operated by Sandia Corporation, a Lockheed Martin Company, for the United States Department of Energy's National Nuclear Security Administration under Contract No. DE-AC04-94-AL85000. The authors are grateful to Dr. S. J. Klippenstein and Dr. L. B. Harding for discussions.

Supporting Information Available: Calculated equilibrium structural parameters of O_2 , OH, H_2O, and HO_2 (Table S1). Minimum energy path for the $H + O_2$ reaction as calculated with the CASPT2 model and several basis sets (Table S2). Effect of inclusion of zero-point vibrational energy along the minimum energy path for the $H + O_2$ reaction (Table S3). Minimum energy path for the $H + OH$ reaction as calculated with the CASPT2 model and several basis sets (Table S4). Effect of inclusion of zero-point vibrational energy along the minimum energy path for the $H + OH$ reaction (Table S5). Potential energy surface for the $H + O_2$ reaction as sampled in the VRC-TST calculation (Figure S1). Falloff curves for the reaction $H + O_2 + M \rightarrow HO_2 + M$ (Figure S2). Effect of spin−orbit coupling along the minimum energy path for the $H + O_2$ reaction (Figure S3). Potential energy surface for the $H + OH$ reaction as sampled in the VRC-TST calculation (Figure S4). Low-pressure limiting rate coefficient as a function of temperature for the reaction $H + OH + N_2$ as calculated using a 2D-ME with LJ parameters of a H-bonded and a T-shaped $H_2O\cdots N_2$ complex (Figure S5). This material is available free of charge via the Internet at http://pubs.acs.org.

References and Notes

(1) Intergovernmental Panel on Climate Change; Climate Change 2007: The Physical Science Basis. Summary for Policymakers; http://www.ipcc.ch. Accessed December 15, 2007.
(2) Li, J.; Zhao, Z. W.; Kazakov, A.; Dryer, F. L. *Int. J. Chem. Kinet.* **2004**, *36*, 566–575.
(3) Ó Conaire, M.; Curran, H. J.; Simmie, J. M.; Pitz, W. J.; Westbrook, C. K. *Int. J. Chem. Kinet* **2004**, *36*, 603–622.
(4) Ströhle, J.; Myhrvold, T. *Int. J. Hydrogen Energ.* **2007**, *32*, 125–135.
(5) Miller, J. A.; Pilling, M. J.; Troe, E. *Proc. Combust. Inst.* **2005**, *30*, 43–88.
(6) Cobos, C. J.; Hippler, H.; Troe, J. *J. Phys. Chem.* **1985**, *89*, 342–349.
(7) Bates, R. W.; Golden, D. M.; Hanson, R. K.; Bowman, C. T. *Phys. Chem. Chem. Phys.* **2001**, *3*, 2337–2342.
(8) Hahn, J.; Krasnoperov, L.; Luther, K.; Troe, J. *Phys. Chem. Chem. Phys* **2004**, *6*, 1997–1999.
(9) Baulch, D. L.; Bowman, C. T.; Cobos, C. J.; Cox, R. A.; Just, T.; Kerr, J. A.; Pilling, M. J.; Stocker, D.; Troe, J.; Tsang, W.; Walker, R. W.; Warnatz, J. *J. Phys. Chem. Ref. Data* **2005**, *34*, 757–1397.
(10) Harding, L. B.; Troe, J.; Ushakov, V. G. *Phys. Chem. Chem. Phys.* **2000**, *2*, 631–642.
(11) Troe, J. *Proc. Combust. Inst.* **2000**, *28*, 1463–1469.
(12) Marques, J. M. C.; Varandas, A. J. C. *Phys. Chem. Chem. Phys.* **2001**, *3*, 505–507.
(13) Harding, L. B.; Troe, J.; Ushakov, V. G. *Phys. Chem. Chem. Phys.* **2001**, *3*, 2630–2631.
(14) Lin, S. Y.; Rackham, E. J.; Guo, H. *J. Phys. Chem. A* **2006**, *110*, 1534–1540.
(15) Pastrana, M. R.; Quintales, L. A. M.; Brandao, J.; Varandas, A. J. C. *J. Phys. Chem.* **1990**, *94*, 8073–8080.
(16) Yang, C.-Y.; Klippenstein, S. J. *J. Chem. Phys.* **1995**, *103*, 7287–7298.
(17) Teitelbaum, H.; Caridade, P. J. S. B.; Varandas, A. J. C. *J. Chem. Phys.* **2004**, *120*, 10483–10500.
(18) Michael, J. V.; Su, M. C.; Sutherland, J. W.; Carroll, J. J.; Wagner, A. F. *J. Phys. Chem. A* **2002**, *106*, 5297–5313.
(19) Himmer, U.; Roduner, E. *Phys. Chem. Chem. Phys.* **2000**, *2*, 339–347.
(20) Duchovic, R. J.; Pettigrew, J. D.; Welling, B.; Shipchandler, T. *J. Chem. Phys.* **1996**, *105*, 10367–10379.
(21) Mandelshtam, V. A.; Taylor, H. S.; Miller, W. H. *J. Chem. Phys.* **1996**, *105*, 496–503.
(22) Troe, J. *J. Chem. Phys.* **1977**, *66*, 4745–4757.
(23) Walch, S. P.; McMichael Rohlfing, C.; Melius, C. F.; Bauschlicher, C. W., Jr. *J. Chem. Phys* **1988**, *88*, 6273–6281.
(24) Walch, S. P.; McMichael Rohlfing, C. *J. Chem. Phys.* **1989**, *91*, 2373–2375.
(25) Walch, S. P.; Duchovic, R. J. *J. Chem. Phys.* **1991**, *94*, 7068–7075.
(26) Ströhle, J.; Myhrvold, T. *Combust. Flame* **2006**, *144*, 545–557.
(27) Srinivasan, N. K.; Michael, J. V. *Int. J. Chem. Kinet.* **2006**, *38*, 211–219.

(28) Walch, S. P.; Harding, L. B. *J. Chem. Phys.* **1988**, *88*, 7653–7661.
(29) Ho, T. S.; Hollebeek, T.; Rabitz, H.; Harding, L. B.; Schatz, G. C. *J. Chem. Phys.* **1996**, *105*, 10472–10486.
(30) Brandao, J.; Rio, C. M. A. *Chem. Phys. Lett.* **2003**, *372*, 866–872.
(31) Brandao, J.; Rio, C. M. A. *J. Chem. Phys.* **2003**, *119*, 3148–3159.
(32) Cobos, C. J.; Troe, J. *J. Chem. Phys.* **1985**, *83*, 1010–1015.
(33) Troe, J. *J. Chem. Phys.* **1977**, *66*, 4758–4775.
(34) Georgievskii, Y.; Klippenstein, S. J. *J. Chem. Phys.* **2003**, *118*, 5442–5455.
(35) Georgievskii, Y.; Klippenstein, S. J. *J. Phys. Chem. A* **2003**, *107*, 9776–9781.
(36) Knowles, P. J.; Werner, H.-J. *Chem. Phys. Lett.* **1985**, *115*, 259–267.
(37) Werner, H.-J.; Knowles, P. J. *J. Chem. Phys.* **1985**, *82*, 5053–5063.
(38) Werner, H. J. *Mol. Phys.* **1996**, *89*, 645–661.
(39) Werner, H. J.; Knowles, P. J. *J. Chem. Phys.* **1988**, *89*, 5803–5814.
(40) Knowles, P. J.; Werner, H. J. *Chem. Phys. Lett.* **1988**, *145*, 514–522.
(41) Werner, H. J.; Knowles, P. J.; Lindh, R.; Manby, F. R.; Schütz, M.; Celani, P.; Korona, T.; Rauhut, G.; Amos, R. D.; Bernhardsson, A.; Berning, A.; Cooper, D. L.; Deegan, M. J. O.; Dobbyn, A. J.; Eckert, F.; Hampel, C.; Hetzer, G.; Lloyd, A. W.; McNicholas, S. J.; Meyer, W.; Mura, M. E.; Nicklass, A.; Palmieri, P.; Pitzer, R.; Schumann, U.; Stoll, H.; Stone, A. J.; Tarroni, R.; Thorsteinsson, T. *MOLPRO, Ver. 2006.1, A Package of Ab Initio Programs*; 2006; http://www.molpro.net.
(42) Becke, A. D. *J. Chem. Phys.* **1993**, *98*, 5648–5652.
(43) Lee, C.; Yang, W.; Parr, R. G. *Phys. Rev. B* **1988**, *37*, 785–789.
(44) Møller, C.; Plesset, M. S. *Phys. Rev.* **1934**, *46*, 618–622.
(45) Raghavachari, K.; Trucks, G. W.; Pople, J. A.; Head-Gordon, M. *Chem. Phys. Lett.* **1989**, *157*, 479–483.
(46) Frisch, M. J.; Trucks, G. W.; Schlegel, H. B.; Scuseria, G. E.; Robb, M. A.; Cheeseman, J. R.; Zakrzewski, V. G.; Montgomery, Jr., J. A.; Stratmann, R. E.; Burant, J. C.; Dapprich, S.; Millam, J. M.; Daniels, A. D.; Kudin, K. N.; Strain, M. C.; Farkas, O.; Tomasi, J.; Barone, V.; Cossi, M.; Cammi, R.; Mennucci, B.; Pomelli, C.; Adamo, C.; Clifford, S.; Ochterski, J.; Petersson, G. A.; Ayala, P. Y.; Cui, Q.; Morokuma, K.; Salvador, P.; Dannenberg, J. J.; Malick, D. K.; Rabuck, A. D.; Raghavachari, K.; Foresman, J. B.; Cioslowski, J.; Ortiz, J. V.; Baboul, A. G.; Stefanov, B. B.; Liu, G.; Liashenko, A.; Piskorz, P.; Komaromi, I.; Gomperts, R.; Martin, R. L.; Fox, D. J.; Keith, T.; Al-Laham, M. A.; Peng, C. Y.; Nanayakkara, A.; Challacombe, M.; Gill, P. M. W.; Johnson, B.; Chen, W.; Wong, M. W.; Andres, J. L.; Gonzalez, C. *Gaussian 98, Revision A.11*; Gaussian, Inc.: Pittsburg, Pennsylvania, 2001.
(47) Schmidt, M. W.; Baldridge, K. K.; Boatz, J. A.; Elbert, S. T.; Gordon, M. S.; Jensen, J. H.; Koseki, S.; Matsunaga, N.; Nguyen, K. A.; Su, S. J.; Windus, T. L.; Dupuis, M.; Montgomery, J. A. *J. Comput. Chem.* **1993**, *14*, 1347–1363.
(48) General Atomic and Molecular Electronic Structure System (GAMESS); http://www.msg.ameslab.gov/GAMESS/GAMESS.html (accessed September 7, 2006).
(49) Dunning, T. H. *J. Chem. Phys.* **1989**, *90*, 1007–1023.
(50) Kendall, R. A.; Dunning, T. H.; Harrison, R. J. *J. Chem. Phys.* **1992**, *96*, 6796–6806.
(51) Woon, D. E.; Dunning, T. H. *J. Chem. Phys.* **1994**, *100*, 2975–2988.
(52) Halkier, A.; Helgaker, T.; Jorgensen, P.; Klopper, W.; Koch, H.; Olsen, J.; Wilson, A. K. *Chem. Phys. Lett.* **1998**, *286*, 243–252.
(53) Wardlaw, D. M.; Marcus, R. A. *J. Phys. Chem.* **1986**, *90*, 5383–5393.
(54) Wardlaw, D. M.; Marcus, R. A. *J. Chem. Phys.* **1985**, *83*, 3462–3480.
(55) Miller, J. A.; Klippenstein, S. J.; Raffy, C. *J. Phys. Chem. A* **2002**, *106*, 4904–4913.
(56) Miller, J. A.; Klippenstein, S. J. *J. Phys. Chem. A* **2004**, *108*, 8296–8306.
(57) Miller, J. A.; Klippenstein, S. J. *J. Phys. Chem. A* **2006**, *110*, 10528–10544.
(58) Klippenstein, S. J.; Wagner, A. F.; Dunbar, R. C.; Wardlaw, D. M.; Robertson, S. H.; Miller, J. A. VARIFLEX Ver. 1.14m; 2005.
(59) Paul, P. H. *DRFM: A New Package for the Evaluation of Gas-phase-transport Properties*; Technical Report SAND98-8203; Sandia National Laboratories, USA, 1997.
(60) Cohen, R. C.; Saykally, R. J. *J. Chem. Phys.* **1993**, *98*, 6007–6030.
(61) Tulegenov, A. S.; Wheatley, R. J.; Hodges, M. P.; Harvey, A. H. *J. Chem. Phys.* **2007**, *126*, 094305.
(62) Ruscic, B.; Wagner, A. F.; Harding, L. B.; Asher, R.; Feller, D.; Dixon, D. A.; Peterson, K. A.; Song, Y.; Qian, X.; Ng, C.-Y.; Liu, J.; Chen, W.; Schwenke, D. W. *J. Phys. Chem. A* **2002**, *106*, 2727–2747.
(63) Ruscic, B.; Pinzon, R. E.; Morton, M. L.; Srinivasan, N. K.; Su, M.-C.; Sutherland, J. W.; Michael, J. V. *J. Phys. Chem. A* **2006**, *110*, 6592–6601.
(64) Johnson III, R. D., Ed. NIST Computational Chemistry Comparison and Benchmark Database, NIST Standard Reference Database Number 101, Release 12;http://srdata.nist.gov/cccbdb, Aug 2005. Accessed December 15, 2007.
(65) Helgaker, T.; Gauss, J.; Jorgensen, P.; Olsen, J. *J. Chem. Phys.* **1997**, *106*, 6430–6440.
(66) Thiesemann, H.; Clifford, E. P.; Taatjes, C. A.; Klippenstein, S. J. *J. Phys. Chem. A* **2001**, *105*, 5393–5401.
(67) Harding, L. B.; Georgievskii, Y.; Klippenstein, S. J. *J. Phys. Chem. A* **2005**, *109*, 4646–4656.
(68) Shepard, R.; Shavitt, I.; Pither, R. M.; Corneau, D. C.; Pepper, M.; Lischka, H.; Szalay, P. G.; Ahlrichs, R.; Brown, F. B.; Zhao, J.-G. *Int. J. Quant. Chem* **1988**, *S22*, 149–165.
(69) Hirao, K. *Chem. Phys. Lett.* **1992**, *190*, 374–380.
(70) Hirao, K. *Chem. Phys. Lett.* **1992**, *196*, 397–403.
(71) Marques, J. M. C.; Varandas, A. J. C. *Phys. Chem. Chem. Phys.* **2001**, *3*, 2632–2633.
(72) Troe, J. *J. Phys. Chem.* **1979**, *83*, 114–126.
(73) Beaudet, R. A.; Poynter, R. L. *J. Phys. Chem. Ref. Data* **1978**, *7*, 311–362.
(74) Celani, P.; Stoll, H.; Werner, H.-J.; Knowles, P. J. *Mol. Phys.* **2004**, *102*, 2369–2379.
(75) Abrams, M. L.; Sherrill, C. D. *J. Phys. Chem. A* **2003**, *107*, 5611–5616.
(76) Klippenstein, S. J.; Georgievskii, Y.; Harding, L. B. *Phys. Chem. Chem. Phys.* **2006**, *8*, 1133–1147.
(77) Sadlej, J.; Rowland, B.; Devlin, J. P.; Buch, V. *J. Chem. Phys.* **1995**, *102*, 4804–4818.
(78) Zellner, R.; Erler, K.; Field, D. *Proc. Combust. Inst.* **1977**, *16*, 939.
(79) Black, G.; Porter, G. *P. Roy. Soc. Lond. A* **1962**, *266*, 185–197.
(80) Marques, J. M. C.; Wang, W.; Pais, A. A. C. C.; Varandas, A. J. C. *J. Phys. Chem.* **1996**, *100*, 17513–17522.
(81) Rodrigues, S. P. J.; Varandas, A. J. C. *J. Phys. Chem. A* **1999**, *103*, 6366–6372.
(82) Ashman, P. J.; Haynes, B. S. *Proc. Combust. Inst.* **1998**, *27*, 185–191.
(83) Carleton, K. L.; Kessler, W. J.; Marinelli, W. J. *J. Phys. Chem.* **1993**, *97*, 6412–6417.
(84) Davidson, D. F.; Petersen, E. L.; Roehrig, M.; Hanson, R. K.; Bowman, C. T. *Proc. Combust. Inst.* **1996**, *26*, 481–488.
(85) Hanning-Lee, M. A.; Pilling, M. J.; Warr, J. F. *J. Chem. Soc., Faraday Trans.* **1991**, *87*, 2907–2912.
(86) Hsu, K. J.; Anderson, S. M.; Durant, J. L.; Kaufman, F. *J. Phys. Chem.* **1989**, *93*, 1018–1021.
(87) Mueller, M. A.; Yetter, R. A.; Dryer, F. L. *Proc. Combust. Inst.* **1998**, *27*, 177–184.
(88) Kurylo, M. J. *J. Phys. Chem.* **1972**, *76*, 3518–3526.
(89) Wong, W.; Davis, D. D. *Int. J. Chem. Kinet.* **1974**, *6*, 401–416.
(90) Friswell, N. J.; Sutton, M. M. *Chem. Phys. Lett.* **1972**, *15*, 108–112.
(91) Gay, A.; Pratt, N. H. In *Proceedings of the 8th International Symposium on Shock Tubes and Waves;* Stollery, J. L., Gaydon, A. G., Owen, P. R., Eds.; Chapman and Hall Ltd.: London, 1971; p. 39/1.
(92) Getzinger, R. W.; Blair, L. S. *Combust. Flame* **1969**, *13*, 271–284.
(93) Goodings, J. M.; Hayhurst, A. N. *J. Chem. Soc., Faraday Trans. 2* **1988**, *84*, 745–762.
(94) Halstead, C. J.; Jenkins, D. R. *Combust. Flame* **1970**, *14*, 321–324.
(95) Halstead, C. J.; Jenkins, D. R. *Proc. Combust. Inst.* **1969**, *12*, 979.
(96) Homer, J. B.; Hurle, I. R. *P. Roy. Soc. Lond. A* **1970**, *314*, 585–598.
(97) Rosenfeld, J. L. J.; Sugden, T. M. *Combust. Flame* **1964**, *8*, 44–50.
(98) Schott, G. L.; Bird, P. F. *J. Chem. Phys.* **1964**, *41*, 2869–2876.

JP711800Z